Environmental Science & Technology

pubs.acs.org/est

Article

Role of Carbonate in Thermodynamic Relationships Describing Pollutant Reduction Kinetics by Iron Oxide-Bound Fe^{2+}

Gongde Chen, Thomas B. Hofstetter, and Christopher A. Gorski*

Cite This: *Environ. Sci. Technol.* 2020, 54, 10109−10117

Read Online

ACCESS | Metrics & More | Article Recommendations | Supporting Information

ABSTRACT: The reduction of environmental pollutants by Fe^{2+} bound to iron oxides is an important process that determines pollutant toxicities and mobilities. Recently, we showed that pollutant reduction rates depend on the thermodynamic driving force of the reaction in a linear free energy relationship that was a function of the solution pH value and the reduction potential, E_H, of the interfacial Fe^{3+}/Fe^{2+} redox couple. In this work, we studied how carbonate affected the free energy relationship by examining the effect that carbonate has on nitrobenzene reduction rates by Fe^{2+} bound to goethite (α-FeOOH). Carbonate slowed nitrobenzene reduction rates by inducing goethite particle aggregation, as evidenced by surface charge and particle size measurements. We observed no evidence for carbonate affecting Fe^{3+}/Fe^{2+} reduction potentials or the mechanism of nitrobenzene reduction. The linear free energy relationship accurately described the data collected in the presence of carbonate when we accounted for the effect it had on the reactive surface area of goethite. The findings from this work provide a framework for determining why common groundwater constituents affect the E_H-dependence of reaction rates involving oxide-bound Fe^{2+} as a reductant.

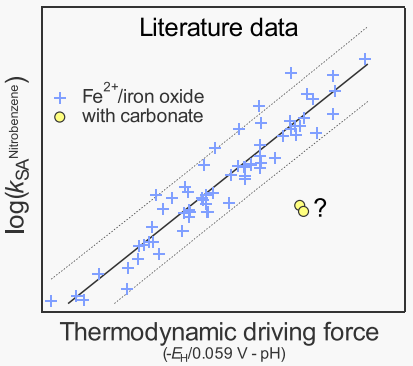

INTRODUCTION

Ferrous iron (Fe^{2+}) can reduce and simultaneously alter the toxicities and/or solubilities of several classes of environmental pollutants found in groundwater.[1−12] Consequently, Fe^{2+} is a critical reductant to account for in naturally attenuated and engineered remediation systems.[13−18] Prior work has established that aqueous Fe^{2+} in the presence of an iron (oxyhydr)oxide (i.e., an "iron oxide") reduces pollutants far more quickly than aqueous Fe^{2+} alone,[2,9,14,19−27] with reduction rates depending on the redox properties of the iron oxide present.[2,4−9,14,16,21,28−41] This effect is a result of the iron oxide influencing what Fe^{3+} oxidation product forms.[28,30,42,43] When aqueous Fe^{2+} is oxidized in the absence of an iron oxide, it tends to form an aqueous Fe^{3+} complex or ferrihydrite.[44] When Fe^{2+} is oxidized in the presence of a crystalline iron oxide, however, it tends to form a more thermodynamically stable iron oxide phase, typically via homoepitaxial growth.[32,45,46] Thus, the presence of an iron oxide alters the reduction potential (E_H) value of the Fe^{3+}/Fe^{2+} redox couple by changing the Fe^{3+} speciation (i.e., the iron oxide that forms).

Recently, we demonstrated that measured E_H values for solutions containing iron oxides and aqueous Fe^{2+} were fully consistent with those calculated from reference thermodynamic values for the Fe^{2+} oxidation and mineral growth process, indicating that thermodynamic calculations can be used to accurately estimate E_H values for suspensions containing iron oxides and aqueous Fe^{2+}.[30] We then showed that the rate constant at which oxide-bound Fe^{2+} reduced organic compounds depended on the thermodynamic driving for Fe^{2+} oxidation, as represented by E_H values of suspensions.[28] Calculated E_H values could be used to construct a linear free energy relationship that correlated reduction rate constants of nitroaromatic compounds by oxide-bound Fe^{2+}, expressed as logarithms of the surface-area-normalized reaction rate constants, $\log(k_{SA})$, to the thermodynamic driving force of the reaction (Section S1, Figure S1A, Table S1)[28]

$$\log(k_{SA}) = a \cdot \frac{E_H}{0.059\text{V}} + b \cdot \text{pH} + c \quad (1)$$

where the E_H term is the reduction potential for the half-reaction of Fe^{2+} oxidation to an iron oxide (shown here for goethite)

$$\alpha - \text{FeOOH}_{(s)} + e^- + 3H^+ \rightleftharpoons Fe^{2+}_{(aq)} + 2H_2O \quad (2)$$

The pH term in eq 1 accounts for the proton transfer step(s) to nitrobenzene at or before the rate-determining step of the reduction pathway. Coefficient c is the y-intercept.[28] The coefficients a and b in eq 1 were both found to be −1 in our prior work,[28] which included data from six independent studies using goethite, hematite, lepidocrocite, ferrihydyrite, and/or magnetite.[9,14,21,28,36,47] The numerical values of these coef-

Received: May 11, 2020
Revised: June 29, 2020
Accepted: July 15, 2020
Published: July 15, 2020

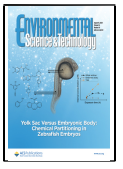

ficients stand for the consensus reaction mechanism in which proton and electron transfers contribute to the rate-limiting step of oxide-bound Fe^{2+} oxidation by nitroaromatic compounds.[28,48−50] Our observation that data for different iron oxides could be fit with a single *c*-term suggested that surface-area normalization of observed rate constants was an adequate procedure to account for reactive oxide-bound Fe^{2+} sites that interact with nitroaromatic compounds.

In the aforementioned studies, the solutions only contained iron oxide particles, aqueous Fe^{2+}, an organic pH buffer, and often a background electrolyte. Interestingly, experiments conducted with additional species commonly found in groundwater (i.e., carbonate, humic acid, or a model humic acid) yielded data that deviate from the free energy relationship in that reaction rate constants were higher and lower than predicted by the calculated E_H of the free energy relationship (eq 1, Figure S1B).[39,51−53] Understanding why these species cause data to diverge from the free energy relationship is an essential step that must be addressed to use the relationship to describe the reactivity of oxide-bound Fe^{2+} in natural and engineered environmental systems. The additional species could alter the free energy relationship in two ways. First, they could change the slope of the free energy relationship (i.e., the *a* and/or *b* terms in eq 1), which represents the relationship between the thermodynamic driving force of the reaction and the reaction rate.[28] This would occur if the species change the reaction mechanism and/or the rate-limiting step of the reaction. Second, the species could alter the y-intercept (i.e., the *c* term in eq 1), which would occur if the species change the number of reactive sites on the iron oxide surface, the frequency of interactions between the electron acceptor and reactive oxide-bound Fe^{2+} sites, and/or the Fe^{2+} oxidation product that forms (due to a change in the standard reduction potential, E^0_H, for the Fe^{3+}/Fe^{2+} half reaction). Unfortunately, data sets, such as those shown in Figure S1B, lack a sufficient amount of information to conclusively discriminate among these possibilities.

The goal of this work was to determine why groundwater constituents cause data to deviate from the generalized linear free energy relationship describing organic compound reduction rates with oxide-bound Fe^{2+}. Specifically, we investigated how and why the presence of carbonate causes data to deviate during the reduction of nitrobenzene by Fe^{2+} bound to goethite. We used nitrobenzene as the model contaminant because it does not sorb or react with iron oxides in the absence of aqueous Fe^{2+}, meaning the nitrobenzene disappearance rate is equal to the reduction rate.[51,54] We focused on carbonate as a model species and examined how it influenced Fe^{2+} uptake, $Fe^{2+}_{(aq)}$/goethite E_H values, goethite aggregation, goethite surface charges, and nitrobenzene reduction rate constants at different pH values. Because equilibrium constants are available to describe complexation reactions between Fe^{2+} and carbonate,[33,55] the collected data allowed us to discriminate among the above hypotheses. That is, we could examine how carbonate influenced the free energy relationship between reaction rate constants and the thermodynamic driving force of the reaction in terms of the slope and y-intercept. We conclude by using these data to offer a more general approach for determining why other groundwater constituents, such as humic acids, alter pollutant reduction rate constants.

MATERIALS AND METHODS

All chemicals were used as purchased, except cyanomethyl viologen, which was synthesized as previously described.[56] All experiments were conducted at room temperature under anaerobic conditions inside a glovebox (MBraun Unilab Workstation, 100% N_2 atmosphere, < 0.1 ppm of O_2). All aqueous solutions were prepared in deionized (DI) water (Millipore Milli-Q system, resistivity >18 MΩ·cm) purged with N_2 (>99.99%) for at least 3 h before being brought into the glovebox.

The pH buffer solutions contained 25 mM KCl and 25 mM pH buffer. The pH buffer used at pH 6.0 and 6.5 was 2-*N*-morpholinoethanesulfonic acid (MES, pK_a 6.1, Aresco, ≥ 99%) and the pH buffer used at pH 7.0 was 3-*N*-morpholinopropanesulfonic acid (MOPS, pK_a 7.2, EMD Chemicals Inc., ≥ 99%). Carbonate stock solutions were freshly made inside the glovebox by dissolving solid $NaHCO_3$ in deoxygenated DI water. The stock solutions were kept in sealed glass vials with little headspace to avoid the loss of carbonate to the N_2 atmosphere. Ferrous chloride ($FeCl_2$, Acros, anhydrous, 99%) was received in a sealed ampule and was transferred to the glovebox to make a 0.2 M aqueous Fe^{2+} stock solution, which was acidified with a few drops of 5 M HCl to avoid inadvertent oxidation. Cyanomethyl viologen was dissolved in deoxygenated DI water to make a 10 mM mediator stock solution. Nitrobenzene (Reagent grade, Sigma-Aldrich) was transferred to a small amber vial with little headspace and taken into the glovebox to make a 10 mM stock solution in deoxygenated methanol.

Goethite Synthesis and Characterization. Goethite was synthesized using an established method.[57] Briefly, 180 mL of 5 M NaOH was added to 100 mL of 0.1 M $Fe(NO_3)_3$ solution with vigorous stirring. The suspension was diluted to 2 L with DI water and heated at 70 °C for 60 h. The produced solid was washed with DI water by centrifugation, freeze-dried, ground in a mortar, and sieved (200 mesh). The crystal phase of the synthesized goethite was confirmed by X-ray diffraction (Malvern Panalytical Empryean) with a Co irradiation source ($K_{\alpha 1}$ = 1.7890 Å, $K_{\alpha 2}$ = 1.7929 Å) operated at 40 kV and 40 mA. All the diffraction peaks (Figure S2) were consistent with goethite (PDF# 29−0713). The specific surface area of the goethite (36 m^2/g) was measured by N_2 sorption isotherms in liquid nitrogen (ASAP 2020 Automated Surface Area and Porosimetry System) and calculated by the multipoint Brunauer−Emmett−Teller (BET) method.[58]

Fe^{2+} Uptake and Mediated Potentiometric Measurements. Fe^{2+} uptake experiments were conducted inside the glovebox by measuring the difference between initial and final aqueous Fe^{2+} concentrations after an equilibration period. The E_H values of $Fe^{2+}_{(aq)}$-goethite suspensions were measured using mediated potentiometry.[30] Specifically, 20 mL aqueous solutions containing 25 mM KCl and 25 mM pH buffer in 20 mL borosilicate glass vials were spiked with the Fe^{2+} stock to make initial Fe^{2+} concentrations ranging from 0.1 to 2.0 mM. For experiments containing carbonate, the solution was spiked with an aliquot of 0.1 or 1 M $NaHCO_3$ stock solution to make the desired concentrations (1 or 10 mM). We chose 10 mM as a maximum carbonate concentration to avoid siderite ($FeCO_{3(s)}$) precipitation ($K_{sp} = 10^{-10.55}$) and to be consistent with past studies.[33,39,59] The pH 6.5 and 7.0 solutions were slightly oversaturated with respect to siderite. We did not observe any loss of Fe^{2+} from solution that could be attributed

https://dx.doi.org/10.1021/acs.est.0c02959
Environ. Sci. Technol. 2020, 54, 10109−10117

to siderite formation in these experiments, consistent with past studies[33,39,59] and recent work that found siderite nucleation did not occur under similar experimental conditions.[59] The solution pH was adjusted to 7.0 using 1 M NaOH or HCl solution. Goethite solid was then added to the reactors to reach a mass loading of 1.0 g/L. The reactors were magnetically stirred. After 1 h, an aliquot of cyanomethyl viologen stock solution was added to make a final mediator concentration of 10 μM. The reactors were sealed with rubber septa and had negligible headspace to prevent carbonate degassing. After being mixed in the dark for 24 h, a small portion of each suspension was filtered through a 0.45 μm nylon syringe filter to measure the final aqueous Fe^{2+} concentration.

The E_H values of $Fe^{2+}_{(aq)}$-goethite suspensions were measured using a Pt redox electrode (Metrohm, part 6.0451.100) inside the glovebox. The data was sampled every 2 s until there was no appreciable change in the measured E_H value over time. The final reading was reported as the E_H value of the suspension. The electrode was periodically cleaned with 0.1 M HCl and calibrated with quinhydrone-saturated pH buffer solutions at pH 4.0 and 7.0.[28,30] All measured E_H values were in reference to AgAgCl, but are reported in reference to the standard hydrogen electrode (SHE) based on the quinhydrone calibration values. The concentrations of total dissolved $Fe^{2+}_{(aq)}$ were measured using the 1,10-phenanthroline method.[60] The speciation of dissolved Fe^{2+} was calculated using the thermodynamic database (thermo.Vdb) in Visual MINTEQ software, v3.1. We manually added equilibria reactions for $Fe(CO_3)(OH)^-$ and $Fe(CO_3)_2^{2-}$, which are not in the MINTEQ database.[33,55] The concentrations of $Fe(H_2O)^{2+}_{6(aq)}$, which we refer to here as "free $Fe^{2+}_{(aq)}$", were calculated using the chemical equilibrium model (Table S2) in Visual MINTEQ software. The activity coefficients of free $Fe^{2+}_{(aq)}$ for each solution were calculated using the Davies model.

Nitrobenzene Reduction Experiments. Nitrobenzene reduction experiments used the same reactor setup as mediated potentiometry measurements, except that no mediator was present. We varied the initial Fe^{2+} concentration (0.2 or 1.0 mM), carbonate concentration (0, 1, or 10 mM), goethite loading (0.25−3 g/L), and solution pH (6.0, 6.5, or 7.0). After a 24 h equilibrium period between the goethite and aqueous Fe^{2+}, a small aliquot was taken to measure the final $Fe^{2+}_{(aq)}$ concentration. Nitrobenzene reduction experiments started with the addition of an aliquot of 10 mM nitrobenzene stock solution made in deoxygenated methanol to make an initial nitrobenzene concentration of ~6 μM. Each reactor was sealed with a Teflon-lined septum and an aluminum crimp cap. At predetermined time intervals, samples were taken and filtered through a 0.2 μm PTFE syringe filter. The sampling volume was minimized to prevent CO_2 loss into the headspace. The concentrations of nitrobenzene and aniline were measured using high pressure liquid chromatograph (HPLC) with a Supelcosil LC-18 column based on a previously established method.[30]

Surface Charge and Particle Size Analysis. The surface charges and aggregate sizes of $Fe^{2+}_{(aq)}$-goethite suspensions were measured by electrophoretic and dynamic light scattering (Malvern Zetasizer Nano ZS), respectively. The reactors were setup as described above, except that no mediator or nitrobenzene was added. The suspensions contained 0.2 mM $Fe^{2+}_{(aq)}$, 1 g/L goethite, 0−10 mM carbonate, 25 mM KCl, and 25 mM pH buffer. We included Fe^{2+} in these measurements because preliminary measurements demonstrated that $Fe^{2+}_{(aq)}$ altered goethite aggregation in the presence of carbonate (data not shown). After a 24 h equilibrium period, a portion of each suspension was transferred to cuvettes or ζ potential cells that were sealed inside the glovebox which were then taken out for subsequent analyses. The intensity weighted mean hydrodynamic diameter was obtained from an autocorrelation function in a digital correlator using the cumulants method.[61] Laser diffraction (Mastersizer 3000) measurements were performed under the same conditions, except that the mass loading of goethite was decreased to 0.05 g/L to meet instrument requirements. The surface-weighted mean diameter was collected based on the Mie scattering model.[62]

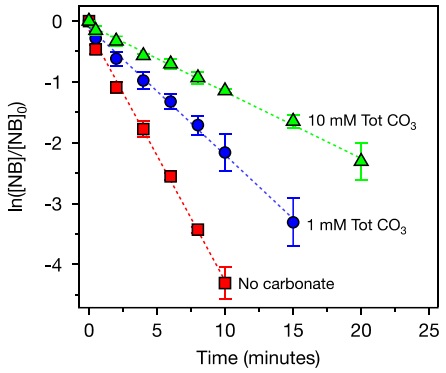

Figure 1. Nitrobenzene (NB) reduction in suspensions containing goethite and aqueous Fe^{2+} at varied total carbonate concentrations. Reactor conditions: 0.2 mM total Fe^{2+}, 0.5 g/L goethite, 25 mM MOPS buffer, 25 mM KCl, and pH = 7.0. The reactors were equilibrated for 24 h prior to the addition of 6 μM nitrobenzene. Error bars represent the two values measured from duplicate reactors, and points represent the average. Straight lines represent the linear fits with pseudo-first-order kinetic model.

RESULTS AND DISCUSSION

Effect of Carbonate on Nitrobenzene Reduction Kinetics. We examined the effect of carbonate on nitrobenzene reduction rates by goethite-bound Fe^{2+} at different pH values, goethite mass loadings, and initial $Fe^{2+}_{(aq)}$ concentrations (Table S3). In all experiments, nitrobenzene disappearance followed pseudo-first-order kinetics, consistent with past studies[28,63]

$$\frac{d[NB]}{dt} = -k_{obs}\cdot[NB] \quad (3)$$

where [NB] is the concentration of nitrobenzene (μM), and k_{obs} is the observed pseudo-first-order reduction rate constant (h^{-1}). The presence of carbonate slowed the rate of nitrobenzene disappearance, with k_{obs} values decreasing from 25.8 ± 0.8 h^{-1} (no carbonate) to 7.1 ± 0.4 h^{-1} (10 mM total carbonate) at pH 7.0, 0.2 mM initial $Fe^{2+}_{(aq)}$, and 0.5 g/L goethite (Figure 1). Nitrobenzene reduction was coupled to aniline production, and a stoichiometric amount of aniline was produced when the reaction was provided sufficient time to proceed to completion (Figure S3). In control experiments lacking goethite, no nitrobenzene disappearance or aniline production occurred over a 24 h period regardless of the carbonate concentration (Figure S4), confirming that goethite-bound Fe^{2+} was the responsible species for nitrobenzene reduction rather than dissolved Fe^{2+} species.[30,64]

https://dx.doi.org/10.1021/acs.est.0c02959
Environ. Sci. Technol. 2020, 54, 10109−10117

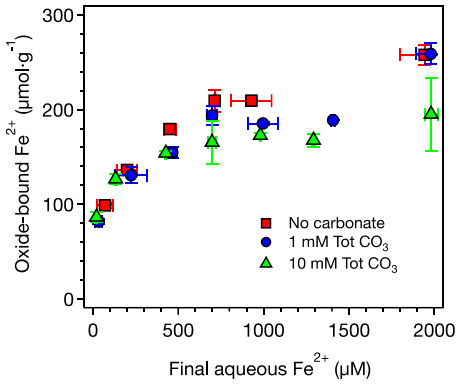

Figure 2. Impact of carbonate on $Fe^{2+}_{(aq)}$ uptake by goethite at pH 7.0 with a 24 h equilibration time. Error bars represent the two values measured from duplicate reactors, and points represent the average. Experimental conditions: 1 g/L goethite, 25 mM KCl, 25 mM MOPS buffer.

We compared measured k_{obs} values with reported values from the literature. In the absence of carbonate, the k_{obs} value (25.8 ± 0.8 h^{-1}), collected with 0.2 mM total Fe^{2+} and 0.5 g/L goethite, agreed well with our previously reported value (32.3 ± 0.7 h^{-1}) collected under similar experimental conditions (0.5 mM total Fe^{2+} and 1 g/L goethite).[28] We previously found this value was consistent with those compiled from several other studies (Figure S1A).[28] In the presence of carbonate, however, our k_{obs} value (7.1 ± 0.4 h^{-1}) was approximately 8 times greater than a value reported in a recent study that used similar experimental conditions with 4-chloronitrobenzene (k_{obs} = 0.96 ± 0.09 h^{-1}).[39] A table detailing the experimental conditions of the two studies is in the Supporting Information (**Table S4**). The substantially larger k_{obs} value in our study was surprising given that the goethite surface area loading and the initial $Fe^{2+}_{(aq)}$ concentration were higher in the cited study[39] (45 m^2/L and 0.5 mM) than in this study (18 m^2/L and 0.2 mM). We examined if this difference was due to the pH buffer (i.e., MOPS) used in our experiments.[31] Our solution contained 25 mM MOPS and 10 mM total carbonate, whereas the former study used only 10 mM total carbonate. When we performed a nitrobenzene reduction experiment without MOPS, the k_{obs} value (6.5 h^{-1}) was similar to what we observed when 25 mM MOPS was present (7.6 h^{-1}) (Figure S5), indicating that the presence of MOPS could not explain the difference in nitrobenzene reduction kinetics. We suspect that the discrepancy in k_{obs} values between the studies may be due to the former study using a much higher initial nitrobenzene concentration (50 μM)[39] than what we used (~6 μM). We observed that high initial nitrobenzene concentrations in the former study prominently decreased the solution pH over the course of the reaction because of insufficient buffer capacity offered by 10 mM carbonate, as 12 protons are generated to completely reduce one nitrobenzene molecule to one aniline molecule by Fe^{2+} bound to goethite.[28]

We explored possible explanations for why carbonate decreased nitrobenzene reduction rates in our experiments. We first examined if carbonate slowed nitrobenzene reduction rates by competing with Fe^{2+} for sorption sites at the goethite surface, as carbonate is known to form surface complexes on goethite at circumneutral pH values.[33,65,66] We compared the extent of Fe^{2+} uptake on the goethite surfaces in the experiments from Figure 1 and in additional experiments with different goethite mass loadings at pH 7.0 (Table S3). The oxide-bound Fe^{2+} loadings for 200 μM initial $Fe^{2+}_{(aq)}$ were indistinguishable at the different total carbonate concentrations (0 mM: 133 ± 54 μmol/g, n = 6; 1 mM: 130 ± 16 μmol/g, n = 6; 10 mM: 132 ± 33 μmol/g, n = 7), indicating that carbonate did not inhibit Fe^{2+} uptake by goethite at 0.2 mM total Fe^{2+}. We did, however, observe that carbonate modestly inhibited Fe^{2+} uptake at higher Fe^{2+} concentrations (≥0.5 mM) at pH 7 (Figure 2). Note a prior study found carbonate significantly inhibited Fe^{2+} sorption on goethite at pH 7.0 under similar goethite surface area loadings and initial Fe^{2+} concentrations.[33] We were unable to reproduce their observation when we replicated their experiment (Figure S6). Unfortunately, we were unable to identify why our results differed from those in the previous work. As a result of our experiments, we ruled out the possibility that nitrobenzene reduction was slowed by carbonate because it inhibited Fe^{2+} uptake (i.e., decreased the number of reactive Fe^{2+} sites), based on the lack of evidence for inhibition at 0.2 mM Fe^{2+}. This finding led us to examine how carbonate influenced E_H values of goethite-bound Fe^{2+}.

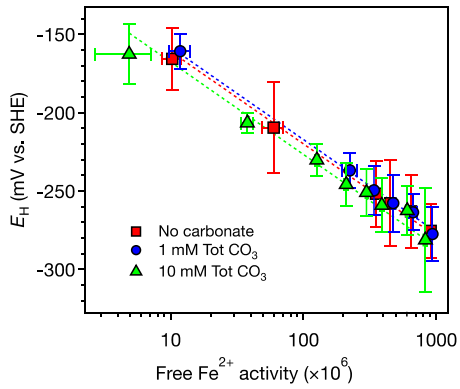

Figure 3. Impact of carbonate on reduction potentials of goethite suspensions as a function of free $Fe^{2+}_{(aq)}$ activity at pH 7.0. Error bars represent the two values measured from duplicate reactors, and points represent the average. Experimental conditions: 1 g/L goethite, 25 mM KCl, 25 mM MOPS buffer, and 10 μM mediator. Dash lines represent data fits using eq 4.

Effect of Carbonate on E_H Values. For each data point in Figure 2, we measured the E_H value of the suspension using mediated potentiometry. Carbonate had a negligible effect on E_H values as a function of the concentration of $Fe(H_2O)^{2+}_{6(aq)}$ (i.e., "free $Fe^{2+}_{(aq)}$") at pH 7 (Figure 3).[28,67,68] Note that we transition here from considering the data in terms of total dissolved Fe^{2+} to free $Fe^{2+}_{(aq)}$ because the Nernst equation requires consideration of a specific Fe^{2+} species. In the presence of carbonate, a portion of the dissolved Fe^{2+} complexes with carbonate to form $Fe(CO_3)(H_2O)^0_{5(aq)}$ (i.e., $FeCO_3^0$) and, to a lesser degree, $Fe(HCO_3)(H_2O)^+_{5(aq)}$ (i.e., $FeHCO_3^+$).[55] In the presence of 10 mM total carbonate at pH 7, approximately 35% of total aqueous Fe^{2+} will be present as $FeCO_3^0$ or $FeHCO_3^+$ (and 3.5% at 1 mM total carbonate), which was calculated based on a chemical equilibrium model (Table S2) in Visual MINTEQ software, V3.1 (Figure S7).[55]

Prior work has shown that aqueous suspensions of goethite and $Fe^{2+}_{(aq)}$ reach thermodynamic equilibrium and can be described by the half reaction shown in eq 2 and the corresponding Nernst equation[30]

$$E_H = E_H^0 - \frac{RT}{F}\ln\{Fe^{2+}_{(aq)}\} + 3\frac{RT}{F}\ln\{H^+\} \quad (4)$$

https://dx.doi.org/10.1021/acs.est.0c02959
Environ. Sci. Technol. 2020, 54, 10109−10117

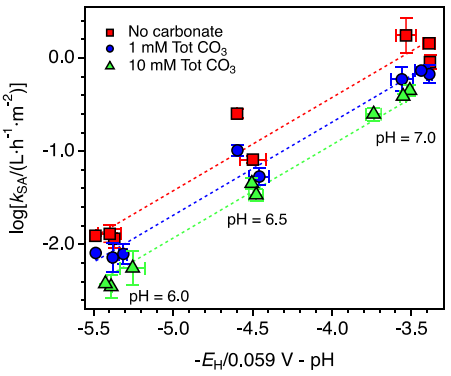

Figure 4. Linear free energy relationship between $\log(k_{SA})$ values and E_H and pH values. The slope of the line was held at 1 during the least-squares linear regression. Error bars represent the two values measured from duplicate reactors, and points represent the average. The dash lines represent the linear fits: r^2 = 0.95 (red), 0.98 (blue), and 0.99 (green).

where $Fe^{2+}_{(aq)}$ is $Fe(H_2O)^{2+}_{6(aq)}$, R is the ideal gas constant, T is temperature, and F is Faraday's constant. At room temperature (298 K), the expression simplifies to

$$E_H = E^0_H - 0.059\ \text{V}{\cdot}\log\{Fe^{2+}_{(aq)}\} - 0.177\ \text{V}{\cdot}\text{pH} \quad (5)$$

Regardless of carbonate concentrations, the measured E_H values were well fit by eq 5 when assuming the theoretical slope value for $Fe^{2+}_{(aq)}$ activity (Figure 3), confirming that goethite and aqueous Fe^{2+} reached thermodynamic equilibrium. Although the free $Fe^{2+}_{(aq)}$ concentration decreases by 35% at 10 mM carbonate because of complexation reactions (Figure S7), calculations based on eq 4 shows that such a change only varies E_H values by 10 mV, which is consistent with minor change in E_H values experimentally observed (Figure 3). The fitted E^0_H values of the α-$FeOOH_{(s)}/Fe^{2+}_{(aq)}$ redox couple in Figure 3 are 783 ± 1 mV vs SHE (no carbonate), 786 ± 1 mV (1 mM total carbonate), and 775 ± 2 mV (10 mM). The values agree well with previously reported values for goethite (800 ± 3 mV[28] and 768 ± 1 mV[30]), indicating that carbonate did not affect the α-$FeOOH_{(s)}/Fe^{2+}_{(aq)}$ half-reaction. We used the average E^0_H value (781 mV) and eq 5 to calculate E_H values in all subsequent experiments.

Relationship between E_H Values and Nitrobenzene Reduction Kinetics. We examined how nitrobenzene reduction kinetics varied as a function of solution E_H and total carbonate concentration (data tabulated in Table S3). We surface-area-normalized the k_{obs} values following a standard convention[28,69,70]

$$k_{SA} = \frac{k_{obs}}{A} \quad (6)$$

where A is the surface area of goethite (m^2/L) in the suspensions, which is calculated by multiplying the goethite BET specific surface area (m^2/g) by the goethite mass loading (g/L). The k_{SA} values consequently have units of $L{\cdot}h^{-1}{\cdot}m^{-2}$. We graphed $\log(k_{SA})$ values as a function of E_H and pH values based on the linear free energy relationship shown in Figure S1A and expressed in eq 1 (Figure 4), with the slope terms (a and b) held constant at −1.[28] Floating both the slopes and y-intercepts during fitting yielded slopes close to 1 (no carbonate: 1.00 ± 0.10, 1 mM total carbonate: 0.99 ± 0.06, 10 mM total carbonate: 1.09 ± 0.02; Figure S8). Note the data points cluster separately with respect to pH because the pH has a substantial impact on the thermodynamic driving force of nitrobenzene reduction by oxide-bound Fe^{2+}.[28] Plotting the data in this way clearly revealed that carbonate did not affect the slope of the free energy relationship, indicating that carbonate did not change the mechanisms and rate-limiting step of the redox reaction between nitrobenzene and oxide-bound Fe^{2+}.[28] We further confirmed that carbonate did not affect the slope in the free energy relationship by performing a 1:1 correlation of $\log(k_{SA})$ values in carbonate-present vs carbonate-free systems, which yielded two straight line with slope values also equal to 1 within error (i.e., 1.02 ± 0.06 and 0.98 ± 0.08, Figure S9).[10]

Carbonate did, however, change the y-intercept of the linear free energy relationship (i.e., the c term in eq 1), with c values lower at higher carbonate concentrations (when the slope was held at 1): 3.57 ± 0.08 (no carbonate), 3.31 ± 0.05 (1 mM total carbonate), and 3.07 ± 0.03 (10 mM). These values reflect an average decrease in k_{SA} by a factor of 1.9 ± 0.8 in 1 mM total carbonate and a factor of 3.3 ± 1.1 in 10 mM total carbonate, relative to 0 mM total carbonate. This trend indicates that carbonate decreased the number of reactive sites and/or the frequency of interactions between nitrobenzene and reactive sites because we did not observe any change in the E^0_H values (Figure 3). This observation led us to determine how carbonate influenced the reactive surface area of goethite by examining its role in particle aggregation.

Role of Carbonate in Goethite Aggregation. To determine if carbonate altered the reactive surface area of goethite, we investigated how the aggregation state of goethite and aqueous Fe^{2+} suspensions changed upon the addition of carbonate. The mean hydrodynamic diameters of goethite aggregates became larger when carbonate was added, as evidenced by dynamic light scattering (DLS) measurements (Figure 5A). At pH 6.0, DLS measurements indicated that the mean hydrodynamic diameter of the goethite aggregates increased from 1.26 ± 0.02 μm (0 mM total carbonate) to 4.8 ± 0.7 μm (10 mM) (Figure 5A). Carbonate also caused goethite to aggregate at pH 6.5 (0 mM: 2.6 ± 0.3 μm, 10 mM: 6.2 ± 0.5 μm) and pH 7.0 (0 mM: 3.6 ± 0.7 μm, 10 mM: 5.5 ± 0.7 μm). Note that calculated hydrodynamic diameters from DLS measurements made at pH 6.5 and 7.0 may have contained some error, as the diameters approached the quantitative detection limit of DLS (~10 μm), and sedimentation was visually apparent during the measurements.[31] Attempts to decrease sedimentation and aggregate sizes by decreasing the goethite loading in solution were unsuccessful (data not shown). Despite the potential for quantitative artifacts in the DLS analyses, the data clearly demonstrated that carbonate increased goethite aggregations.

We also measured goethite aggregation state using laser diffraction, which has a wider detection range (10 nm −3500 μm),[62] but requires the samples to be exposed to air during analysis. These measurements confirmed that carbonate induced aggregation (Figure S10). At pH 6.0, the mean diameter of goethite aggregates increased from 2.4 ± 0.1 (0 mM total carbonate) to 5.0 ± 0.1 μm (10 mM total carbonate), consistent with the DLS results. Similarly, laser diffractions measurements also indicated that carbonate induced goethite aggregation at pH 6.5 (0 mM: 3.3 ± 0.1, 10 mM: 4.9 ± 0.1) and pH 7.0 (0 mM: 3.0 ± 0.2 μm, 10 mM: 4.3 ± 0.1 μm), although the magnitude of the effect was smaller than what we measured with DLS. We suspect the laser

https://dx.doi.org/10.1021/acs.est.0c02959
Environ. Sci. Technol. 2020, 54, 10109−10117

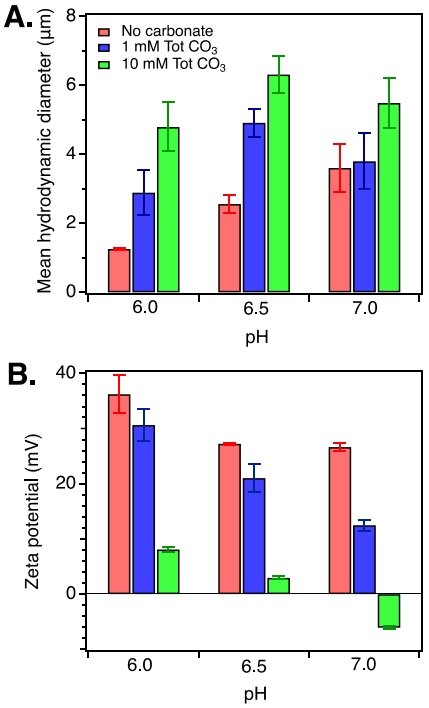

Figure 5. Impact of carbonate on the mean hydrodynamic diameters (A) and ζ potentials (B) of goethite in the presence of $Fe^{2+}_{(aq)}$ at different pH values. Error bars represent standard deviations from triplicate measurements. Experimental conditions: 1 g/L goethite, 0.2 mM $Fe^{2+}_{(aq)}$, 25 mM KCl, and 25 mM MES or MOPS buffer.

diffraction measurements may have been affected by Fe^{2+} oxidation due to air exposure during analysis. Prior work found that Fe^{2+} oxidation by oxygen changes the surface charge and aggregation states of goethite.[39]

We examined if the reason carbonate increased goethite aggregation was that it formed surface complexes on the goethite surface that altered the particles' surface charge.[33,71] We tested this hypothesis by performing ζ potential measurements on the suspensions used for DLS experiments (Figure 5B). Over pH 6.0 to 7.0, carbonate lowered the surface charge of goethite, bringing it closer to zero thus favoring particle aggregation by decreasing interparticle repulsive forces. The point of zero charge of goethite has been reported to be approximately 9.0,[72] but the presence of 10 mM carbonate lowered it to a value between 6.5 to 7.0 (Figure 5B). Prior work has reported the following inner-sphere surface complexation reactions of carbonate interacting with goethite surfaces[33]

$$\equiv FeOH + CO_3^{2-} + H^+ \rightleftharpoons \equiv FeO^{-0.2}COO^{-0.8} + H_2O \log(K) = 12.76 \quad (7)$$

$$\equiv FeOH + CO_3^{2-} + 2H^+ \rightleftharpoons \equiv FeOCOOH + H_2O \log(K) = 18.29 \quad (8)$$

In addition, carbonate likely formed outer-sphere complexes in the double layer of goethite particles through electrostatic interaction and neutralized positively charged goethite surface. Our results are consistent with carbonate forming surface complexes on goethite and inducing aggregation, yet interestingly, our earlier results in Figure 2 indicated that Fe^{2+} and carbonate did not compete for sorption sites with 0.2 mM total Fe^{2+}. Given the strong evidence for interfacial electron-transfer between Fe^{2+} and iron oxides, we speculate that this observation may be a result of Fe^{2+} uptake extent being controlled by the redox properties of the iron oxide as opposed to surface complexation associated with the number of surface sites.[71−73]

Correcting the Reactive Surface Area of Goethite. As discussed above, the linear free energy relationships in Figure 4 were developed using a k_{SA} value that was calculated based on the BET surface area of dry goethite (eq 5). However, the actual reactive surface area of goethite in aqueous suspensions appeared to vary with respect to the total carbonate concentration due to aggregation. To account for aggregation in the free energy relationship, we normalized nitrobenzene reduction rate constant (k_{obs}) with the calculated goethite specific surface area in aqueous suspension from DLS and laser diffraction measurements. This normalization required us to make an approximation that the goethite aggregates, which likely consisted of loosely and irregularly bound rod-shaped particles,[38] could be described as spherical particles. This approximation would be valid if the actual reactive surface area of the aggregate is linearly proportional to the calculated surface area when assuming the aggregates are spherical. Using this approximation, we calculated the geometric specific surface area (SSA_{aq}) based on the mean diameters (d) of equivalent spheres of goethite[73,74]

$$SSA_{aq} = \frac{4\pi\left(\frac{d}{2}\right)^2}{\rho\frac{4}{3}\pi\left(\frac{d}{2}\right)^3} = \frac{6}{\rho d} \quad (9)$$

where ρ represents the density of goethite (4.26 g/cm^3).[75] The calculated SSA_{aq} values from DLS and laser diffraction ranged from 0.21 to 1.13 m^2/g, depending on the pH and total carbonate concentrations. The SSA_{aq} values were much lower than the BET specific surface area value measured for the dry particles (36 m^2/g), which was likely due to the aggregation and our simplistic approximation that the aggregates were spherical.

We then readjusted our linear free energy relationship by calculating the logarithm of the calibrated surface-area-normalized reaction rate constant ($\log[k'_{SA}]$)

$$\log(k'_{SA}) = \log\left(\frac{k_{obs}}{SSA_{aq}\cdot m_L}\right) \quad (10)$$

where m_L is mass loading (g/L) of goethite. We graphed $\log(k'_{SA})$ values as a function of E_H and pH values based on the linear free energy relationship (eq 1). After the calibration based on DLS results, the scattered data points in Figure 4 closely converged for different carbonate concentrations (Figure 6), which was quantitatively reflected by the similarity among the fitted y-intercepts (c term): 5.29 ± 0.10 (0 mM), 5.25 ± 0.04 (1 mM), and 5.19 ± 0.04 (10 mM). Calibration based on laser diffraction results also highly reduced scatter among the data (Figure S11), although they converged to a lesser extent. These results indicate that the loss of the reactive surface area due to goethite aggregation was the primary reason that nitrobenzene reduction slowed in the presence of carbonate. Therefore, we concluded that the main mechanism by which carbonate slows nitrobenzene reduction by Fe^{2+}-bound to goethite is via particle aggregation caused by carbonate forming surface complexes on the goethite surface that decrease the positive surface charge of goethite.

https://dx.doi.org/10.1021/acs.est.0c02959
Environ. Sci. Technol. 2020, 54, 10109−10117

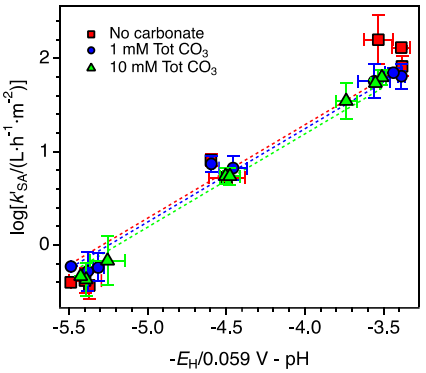

Figure 6. Impact of carbonate on the logarithms of the calibrated surface-area-normalized reaction rate constants ($\log(k'_{SA})$) based on DLS results as a function of E_H and pH values of $Fe^{2+}_{(aq)}$-goethite suspension for nitrobenzene reduction. Dashed lines represent the linear fits: r^2 = 0.94 (red), 0.98 (blue), and 0.99 (green). The slopes were held at 1 during fitting. When the slopes were allowed to float, they reached values close to 1, with the small deviations attributed to experimental error.

Environmental Implications. Our results indicate that the predominant way in which carbonate alters the reduction rates of nitroaromatic compounds by oxide-bound Fe^{2+} is by changing particulate aggregation state. Carbonate increased goethite aggregation, which decreased the number of reactive sites on goethite surfaces. We did not observe any evidence suggesting that carbonate affected the nitrobenzene reduction mechanism, which would have changed the slope of the linear free energy relationship. The effect that carbonate has on iron oxide particle aggregation will be highly specific to the iron oxide present because aggregation behavior depends on the point of zero charge of an iron oxides, which is oxide-specific.[75] Reported point of zero charge values for goethite range between 8.9−9.4.[75] Other iron oxides have far lower point of zero charges, such as magnetite (6.3−7.1) and lepidocrocite (6.7−7.45).[75] Given the differences in point of zero charge, iron oxides likely have distinctive surface charges under environmentally relevant conditions, which affect surface complexation of carbonate on iron oxides. Consequently, carbonate will likely affect their aggregation behavior differently.

More generally, our results offer evidence to support the use of free energy relationships to understand how groundwater constituents alter pollutant reduction rates by oxide-bound Fe^{2+} mechanistically. By constructing a free energy relationship that relates reduction rates to the thermodynamic driving force of the reaction, one can differentiate between how a groundwater constituent may change a reaction pathway (as evidenced by a change in the slope of the relationship) or how it changes the number of reactive sites or the Fe^{2+} oxidation product that is formed (as evidenced by a change to the y-intercept). Coupling this analysis with E_H measurements could, for example, allow one to discriminate among possible reasons that humic acids alter nitroaromatic reduction rates by oxide-bound Fe^{2+}, which has proven to be a difficult task.[51−53] Humic acid may alter pollutant reduction rates by aggregating particles,[38,76] complexing aqueous Fe^{2+},[77,78] changing Fe^{2+} oxidation products,[77] and/or by serving as electron shuttles.[51] Coupling E_H measurements with conventionally used approaches may allow researchers to discriminate among these possibilities for other classes of contaminants as well, as was recently shown for chlorinated solvents reacted with reduced natural sediments.[16]

■ ASSOCIATED CONTENT

Supporting Information

The Supporting Information is available free of charge at https://pubs.acs.org/doi/10.1021/acs.est.0c02959.

Compiled data from the literature, the XRD pattern of goethite, the impact of carbonate on E_H values, the goethite particle sizes and nitrobenzene reduction, the impact of MOPS buffer on nitrobenzene reduction, and the predominance diagrams of Fe^{2+} species (PDF)

■ AUTHOR INFORMATION

Corresponding Author

Christopher A. Gorski − *Department of Civil & Environmental Engineering, Pennsylvania State University, University Park, Pennsylvania 16802, United States;* orcid.org/0000-0002-5363-2904; Phone: (814) 865-5673; Email: gorski@psu.edu; Fax: (814) 863-7304

Authors

Gongde Chen − *Department of Civil & Environmental Engineering, Pennsylvania State University, University Park, Pennsylvania 16802, United States;* orcid.org/0000-0002-7725-1698

Thomas B. Hofstetter − *Eawag, Swiss Federal Institute of Aquatic Science and Technology, Dübendorf 8600, Switzerland; Institute of Biogeochemistry and Pollutant Dynamics (IBP), Swiss Federal Institute of Technology, ETH Zürich, Zürich 8092, Switzerland;* orcid.org/0000-0003-1906-367X

Complete contact information is available at: https://pubs.acs.org/10.1021/acs.est.0c02959

Notes

The authors declare no competing financial interest.

■ ACKNOWLEDGMENTS

The study was supported by U.S. National Science Foundation Program (CHE-1807703 to CAG) and the Swiss National Science Foundation (Grant 200021_149283 to TBH). Any opinions, findings, and conclusions or recommendations expressed in this material are those of the authors and do not necessarily reflect the views of the National Science Foundation.

■ REFERENCES

(1) Eary, L.; Rai, D. Chromate removal from aqueous wastes by reduction with ferrous ion. *Environ. Sci. Technol.* **1988**, *22* (8), 972−977.

(2) Buerge, I. J.; Hug, S. J. Influence of mineral surfaces on chromium (VI) reduction by iron (II). *Environ. Sci. Technol.* **1999**, *33* (23), 4285−4291.

(3) Latta, D. E.; Gorski, C. A.; Boyanov, M. I.; O'Loughlin, E. J.; Kemner, K. M.; Scherer, M. M. Influence of magnetite stoichiometry on UVI reduction. *Environ. Sci. Technol.* **2012**, *46* (2), 778−786.

(4) Myneni, S. C. B.; Tokunaga, T. K.; Brown, G. Abiotic selenium redox transformations in the presence of Fe (II, III) oxides. *Science* **1997**, *278* (5340), 1106−1109.

(5) Amonette, J. E.; Workman, D. J.; Kennedy, D. W.; Fruchter, J. S.; Gorby, Y. A. Dechlorination of carbon tetrachloride by Fe (II) associated with goethite. *Environ. Sci. Technol.* **2000**, *34* (21), 4606−4613.

(6) Pecher, K.; Haderlein, S. B.; Schwarzenbach, R. P. Reduction of polyhalogenated methanes by surface-bound Fe (II) in aqueous suspensions of iron oxides. *Environ. Sci. Technol.* **2002**, *36* (8), 1734−1741.
(7) Strathmann, T. J.; Stone, A. T. Mineral surface catalysis of reactions between FeII and oxime carbamate pesticides. *Geochim. Cosmochim. Acta* **2003**, *67* (15), 2775−2791.
(8) Li, X.; Chen, Y.; Zhang, H. Reduction of nitrogen-oxygen containing compounds (NOCs) by surface-associated Fe (II) and comparison with soluble Fe (II) complexes. *Chem. Eng. J.* **2019**, *370*, 782−791.
(9) Elsner, M.; Schwarzenbach, R. P.; Haderlein, S. Reactivity of Fe(II)-Bearing Minerals toward Reductive Transformation of Organic Contaminants. *Environ. Sci. Technol.* **2004**, *38*, 799−807.
(10) Tratnyek, P. G.; Weber, E. J.; Schwarzenbach, R. P. Quantitative structure-activity relationships for chemical reductions of organic contaminants. *Environ. Toxicol. Chem.* **2003**, *22* (8), 1733−1742.
(11) Amstaetter, K.; Borch, T.; Larese-Casanova, P.; Kappler, A. Redox transformation of arsenic by Fe (II)-activated goethite (α-FeOOH). *Environ. Sci. Technol.* **2010**, *44* (1), 102−108.
(12) Jeon, B.-H.; Dempsey, B. A.; Burgos, W. D.; Barnett, M. O.; Roden, E. E. Chemical reduction of U (VI) by Fe (II) at the solid−water interface using natural and synthetic Fe (III) oxides. *Environ. Sci. Technol.* **2005**, *39* (15), 5642−5649.
(13) Melton, E. D.; Swanner, E. D.; Behrens, S.; Schmidt, C.; Kappler, A. The interplay of microbially mediated and abiotic reactions in the biogeochemical Fe cycle. *Nat. Rev. Microbiol.* **2014**, *12* (12), 797−808.
(14) Fan, D.; Bradley, M. J.; Hinkle, A. W.; Johnson, R. L.; Tratnyek, P. G. Chemical reactivity probes for assessing abiotic natural attenuation by reducing iron minerals. *Environ. Sci. Technol.* **2016**, *50* (4), 1868−1876.
(15) Bussan, A. L.; Strathmann, T. J. Influence of organic ligands on the reduction of polyhalogenated alkanes by iron (II). *Environ. Sci. Technol.* **2007**, *41* (19), 6740−6747.
(16) Kocur, C. M.; Fan, D.; Tratnyek, P. G.; Johnson, R. L., Predicting Abiotic Reduction Rates Using Cryogenically Collected Soil Cores and Mediated Reduction Potential Measurements. *Environ. Sci. Technol. Lett.* **2020**.720
(17) Wilkin, R. T.; Su, C.; Ford, R. G.; Paul, C. J. Chromium-removal processes during groundwater remediation by a zerovalent iron permeable reactive barrier. *Environ. Sci. Technol.* **2005**, *39* (12), 4599−4605.
(18) Liang, S.; Kao, C.; Kuo, Y.; Chen, K.; Yang, B. In situ oxidation of petroleum-hydrocarbon contaminated groundwater using passive ISCO system. *Water Res.* **2011**, *45* (8), 2496−2506.
(19) Amonette, J. E.; Workman, D. J.; Kennedy, D. W.; Fruchter, J. S.; Gorby, Y. A. Dechlorination of Carbon Tetrachloride by Fe(II) Associated with Goethite. *Environ. Sci. Technol.* **2000**, *34* (21), 4606−4613.
(20) Strathmann, T. J.; Stone, A. T. Mineral surface catalysis of reactions between Fe(II) and oxime carbamate pesticides. *Geochim. Cosmochim. Acta* **2003**, *67* (15), 2775−2791.
(21) Klausen, J.; Trober, S. P.; Haderlein, S. B.; Schwarzenbach, R. P. Reduction of substituted nitrobenzenes by Fe(II) in aqueous mineral suspensions. *Environ. Sci. Technol.* **1995**, *29* (9), 2396−2404.
(22) Rügge, K.; Hofstetter, T. B.; Haderlein, S. B.; Bjerg, P. L.; Knudsen, S.; Zraunig, C.; Mosbæk, H.; Christensen, T. H. Characterization of Predominant Reductants in an Anaerobic Leachate-Contaminated Aquifer by Nitroaromatic Probe Compounds. *Environ. Sci. Technol.* **1998**, *32* (1), 23−31.
(23) Pecher, K.; Haderlein, S. B.; Schwarzenbach, R. P. Reduction of polyhalogenated methanes by surface-bound Fe(II) in aqueous suspensions of iron oxides. *Environ. Sci. Technol.* **2002**, *36* (8), 1734−1741.
(24) Cui, D.; Eriksen, T. E. Reduction of pertechnetate by ferrous iron in solution: Influence of sorbed and precipitated Fe (II). *Environ. Sci. Technol.* **1996**, *30* (7), 2259−2262.
(25) Liger, E.; Charlet, L.; Van Cappellen, P. Surface catalysis of uranium(VI) reduction by iron(II). *Geochim. Cosmochim. Acta* **1999**, *63* (19−20), 2939−2955.
(26) Colón, D.; Weber, E. J.; Anderson, J. L. QSAR Study of the Reduction of Nitroaromatics by Fe(II) Species. *Environ. Sci. Technol.* **2006**, *40* (16), 4976−4982.
(27) Jones, A. M.; Kinsela, A. S.; Collins, R. N.; Waite, T. D. The reduction of 4-chloronitrobenzene by Fe(II)-Fe(III) oxide systems - correlations with reduction potential and inhibition by silicate. *J. Hazard. Mater.* **2016**, *320*, 143−149.
(28) Stewart, S. M.; Hofstetter, T. B.; Joshi, P.; Gorski, C. A. Linking thermodynamics to pollutant reduction kinetics by Fe^{2+} bound to iron oxides. *Environ. Sci. Technol.* **2018**, *52* (10), 5600−5609.
(29) Strehlau, J. H.; Schultz, J. D.; Vindedahl, A. M.; Arnold, W. A.; Penn, R. L. Effect of nonreactive kaolinite on 4-chloronitrobenzene reduction by Fe (II) in goethite−kaolinite heterogeneous suspensions. *Environ. Sci.: Nano* **2017**, *4* (2), 325−334.
(30) Gorski, C. A.; Edwards, R.; Sander, M.; Hofstetter, T. B.; Stewart, S. M. Thermodynamic characterization of iron oxide−aqueous Fe^{2+} redox couples. *Environ. Sci. Technol.* **2016**, *50* (16), 8538−8547.
(31) Stemig, A. M.; Do, T. A.; Yuwono, V. M.; Arnold, W. A.; Penn, R. L. Goethite nanoparticle aggregation: effects of buffers, metal ions, and 4-chloronitrobenzene reduction. *Environ. Sci.: Nano* **2014**, *1* (5), 478−487.
(32) Chun, C. L.; Penn, R. L.; Arnold, W. A. Kinetic and microscopic studies of reductive transformations of organic contaminants on goethite. *Environ. Sci. Technol.* **2006**, *40* (10), 3299−3304.
(33) Vikesland, P. J.; Valentine, R. L. Iron oxide surface-catalyzed oxidation of ferrous iron by monochloramine: Implications of oxide type and carbonate on reactivity. *Environ. Sci. Technol.* **2002**, *36* (3), 512−519.
(34) Liger, E.; Charlet, L.; Van Cappellen, P. Surface catalysis of uranium (VI) reduction by iron (II). *Geochim. Cosmochim. Acta* **1999**, *63* (19−20), 2939−2955.
(35) Hofstetter, T. B.; Heijman, C. G.; Haderlein, S. B.; Holliger, C.; Schwarzenbach, R. P. Complete reduction of TNT and other (poly) nitroaromatic compounds under iron-reducing subsurface conditions. *Environ. Sci. Technol.* **1999**, *33* (9), 1479−1487.
(36) Jones, A. M.; Kinsela, A. S.; Collins, R. N.; Waite, T. D. The reduction of 4-chloronitrobenzene by Fe (II)-Fe (III) oxide systems-correlations with reduction potential and inhibition by silicate. *J. Hazard. Mater.* **2016**, *320*, 143−149.
(37) Vindedahl, A. M.; Strehlau, J. H.; Arnold, W. A.; Penn, R. L. Organic matter and iron oxide nanoparticles: aggregation, interactions, and reactivity. *Environ. Sci.: Nano* **2016**, *3* (3), 494−505.
(38) Vindedahl, A. M.; Stemig, M. S.; Arnold, W. A.; Penn, R. L. Character of humic substances as a predictor for goethite nanoparticle reactivity and aggregation. *Environ. Sci. Technol.* **2016**, *50* (3), 1200−1208.
(39) Strehlau, J. H.; Stemig, M. S.; Penn, R. L.; Arnold, W. A. Facet-dependent oxidative goethite growth as a function of aqueous solution conditions. *Environ. Sci. Technol.* **2016**, *50* (19), 10406−10412.
(40) Huang, J.; Wang, Q.; Wang, Z.; Zhang, H. Interactions and reductive reactivity in ternary mixtures of Fe (II), goethite, and phthalic acid based on a combined experimental and modeling approach. *Langmuir* **2019**, *35* (25), 8220−8227.
(41) Huang, J.; Dai, Y.; Liu, C.-C.; Zhang, H. Effects of Second Metal Oxides on Surface-Mediated Reduction of Contaminants by Fe (II) with Iron Oxide. *ACS Earth and Space Chemistry* **2019**, *3* (5), 680−687.
(42) Felmy, A. R.; Moore, D. A.; Rosso, K. M.; Qafoku, O.; Rai, D.; Buck, E. C.; Ilton, E. S. Heterogeneous reduction of PuO_2 with Fe (II): Importance of the Fe (III) reaction product. *Environ. Sci. Technol.* **2011**, *45* (9), 3952−3958.
(43) Felmy, A. R.; Ilton, E. S.; Rosso, K. M.; Zachara, J. M. Interfacial reactivity of radionuclides: emerging paradigms from molecular-level observations. *Mineral. Mag.* **2011**, *75* (4), 2379−2391.

https://dx.doi.org/10.1021/acs.est.0c02959
Environ. Sci. Technol. 2020, 54, 10109−10117

(44) Schwertmann, U.; Carlson, L.; Fechter, H. Iron oxide formation in artificial ground waters. *Schweiz. Z. Hydrol.* **1984**, *46* (2), 185−191.
(45) Larese-Casanova, P.; Kappler, A.; Haderlein, S. B. Heterogeneous Oxidation of Fe(II) on Iron Oxides in Aqueous Systems: Identification and Controls of Fe(III) Product Formation. *Geochim. Cosmochim. Acta* **2012**, *91*, 171−186.
(46) Jones, A. M.; Griffin, P. J.; Collins, R. N.; Waite, T. D. Ferrous iron oxidation under acidic conditions−The effect of ferric oxide surfaces. *Geochim. Cosmochim. Acta* **2014**, *145*, 1−12.
(47) Colón, D.; Weber, E. J.; Anderson, J. L. QSAR study of the reduction of nitroaromatics by Fe (II) species. *Environ. Sci. Technol.* **2006**, *40* (16), 4976−4982.
(48) Hartenbach, A. E.; Hofstetter, T. B.; Aeschbacher, M.; Sander, M.; Kim, D.; Strathmann, T. J.; Arnold, W. A.; Cramer, C. J.; Schwarzenbach, R. P. Variability of nitrogen isotope fractionation during the reduction of nitroaromatic compounds with dissolved reductants. *Environ. Sci. Technol.* **2008**, *42* (22), 8352−8359.
(49) Hartenbach, A.; Hofstetter, T. B.; Berg, M.; Bolotin, J.; Schwarzenbach, R. P. Using nitrogen isotope fractionation to assess abiotic reduction of nitroaromatic compounds. *Environ. Sci. Technol.* **2006**, *40* (24), 7710−7716.
(50) Hofstetter, T. B.; Neumann, A.; Arnold, W. A.; Hartenbach, A. E.; Bolotin, J.; Cramer, C. J.; Schwarzenbach, R. P. Substituent effects on nitrogen isotope fractionation during abiotic reduction of nitroaromatic compounds. *Environ. Sci. Technol.* **2008**, *42* (6), 1997−2003.
(51) Colón, D.; Weber, E. J.; Anderson, J. L. Effect of natural organic matter on the reduction of nitroaromatics by Fe (II) species. *Environ. Sci. Technol.* **2008**, *42* (17), 6538−6543.
(52) Luan, F.; Xie, L.; Li, J.; Zhou, Q. Abiotic reduction of nitroaromatic compounds by Fe(II) associated with iron oxides and humic acid. *Chemosphere* **2013**, *91* (7), 1035−1041.
(53) Huang, J.; Cao, J.; Tu, N.; Dong, H.; Li, J.; Shou, J.; Li, Y. Effect of surfactants on the removal of nitrobenzene by Fe-bearing montmorillonite/Fe (II). *J. Colloid Interface Sci.* **2019**, *533*, 409−415.
(54) Cao, J.; Huang, J.; Dong, H.; Li, J.; Shou, J.; Li, Y. Effects of surfactants on the removal of nitrobenzene by Fe (II) sorbed on goethite. *J. Colloid Interface Sci.* **2019**, *552*, 764−770.
(55) King, D. W. Role of carbonate speciation on the oxidation rate of Fe (II) in aquatic systems. *Environ. Sci. Technol.* **1998**, *32* (19), 2997−3003.
(56) Gorski, C. A.; Klüpfel, L.; Voegelin, A.; Sander, M.; Hofstetter, T. B. Redox properties of structural Fe in clay minerals. 2. Electrochemical and spectroscopic characterization of electron transfer irreversibility in ferruginous smectite, SWa-1. *Environ. Sci. Technol.* **2012**, *46* (17), 9369−9377.
(57) Schwertmann, U.; Cornell, R. M. *Iron oxides in the laboratory: preparation and characterization*. John Wiley & Sons: 2008.
(58) Brunauer, S.; Emmett, P. H.; Teller, E. Adsorption of gases in multimolecular layers. *J. Am. Chem. Soc.* **1938**, *60* (2), 309−319.
(59) Jiang, C. Z.; Tosca, N. J. Fe (II)-carbonate precipitation kinetics and the chemistry of anoxic ferruginous seawater. *Earth Planet. Sci. Lett.* **2019**, *506*, 231−242.
(60) Tamura, H.; Goto, K.; Yotsuyanagi, T.; Nagayama, M. Spectrophotometric determination of iron (II) with 1, 10-phenanthroline in the presence of large amounts of iron (III). *Talanta* **1974**, *21* (4), 314−318.
(61) Koppel, D. E. Analysis of macromolecular polydispersity in intensity correlation spectroscopy: the method of cumulants. *J. Chem. Phys.* **1972**, *57* (11), 4814−4820.
(62) Malvern Instruments Ltd, M., Mastersizer 3000 User Manual. 2015.
(63) Gorski, C. A.; Nurmi, J. T.; Tratnyek, P. G.; Hofstetter, T. B.; Scherer, M. M. Redox behavior of magnetite: Implications for contaminant reduction. *Environ. Sci. Technol.* **2010**, *44* (1), 55−60.
(64) Huang, J.; Wang, Q.; Wang, Z.; Zhang, H. J., Interactions and Reductive Reactivity in Ternary Mixtures of Fe (II), Goethite, and Phthalic Acid based on a Combined Experimental and Modeling Approach. *Langmuir* **2019**. DOI: 10.1021/acs.langmuir.9b00538
(65) Villalobos, M.; Leckie, J. O. Surface complexation modeling and FTIR study of carbonate adsorption to goethite. *J. Colloid Interface Sci.* **2001**, *235* (1), 15−32.
(66) van Geen, A.; Robertson, A. P.; Leckie, J. O. Complexation of carbonate species at the goethite surface: Implications for adsorption of metal ions in natural waters. *Geochim. Cosmochim. Acta* **1994**, *58* (9), 2073−2086.
(67) Sander, M.; Hofstetter, T. B.; Gorski, C. A. Electrochemical analyses of redox-active iron minerals: a review of nonmediated and mediated approaches. *Environ. Sci. Technol.* **2015**, *49* (10), 5862−5878.
(68) Gorski, C. A.; Aeschbacher, M.; Soltermann, D.; Voegelin, A.; Baeyens, B.; Marques Fernandes, M.; Hofstetter, T. B.; Sander, M. Redox properties of structural Fe in clay minerals. 1. Electrochemical quantification of electron-donating and-accepting capacities of smectites. *Environ. Sci. Technol.* **2012**, *46* (17), 9360−9368.
(69) Arnold, W. A.; Roberts, A. L. Pathways and kinetics of chlorinated ethylene and chlorinated acetylene reaction with Fe (0) particles. *Environ. Sci. Technol.* **2000**, *34* (9), 1794−1805.
(70) Scherer, M. M.; Balko, B. A.; Gallagher, D. A.; Tratnyek, P. G. Correlation analysis of rate constants for dechlorination by zero-valent iron. *Environ. Sci. Technol.* **1998**, *32* (19), 3026−3033.
(71) Villalobos, M.; Trotz, M. A.; Leckie, J. O. Surface complexation modeling of carbonate effects on the adsorption of Cr (VI), Pb (II), and U (VI) on goethite. *Environ. Sci. Technol.* **2001**, *35* (19), 3849−3856.
(72) Villalobos, M.; Leckie, J. O. Carbonate adsorption on goethite under closed and open CO_2 conditions. *Geochim. Cosmochim. Acta* **2000**, *64* (22), 3787−3802.
(73) White, A. F.; Peterson, M. L. *Role of reactive-surface-area characterization in geochemical kinetic models*. In ACS Publications: 1990.
(74) Liu, J.; Aruguete, D. M.; Murayama, M.; Hochella, M. F., Jr Influence of size and aggregation on the reactivity of an environmentally and industrially relevant nanomaterial (PbS). *Environ. Sci. Technol.* **2009**, *43* (21), 8178−8183.
(75) Cornell, R. M.; Schwertmann, U. *The iron oxides: structure, properties, reactions, occurrences and uses*. John Wiley & Sons: 2003.
(76) Baalousha, M. Aggregation and disaggregation of iron oxide nanoparticles: influence of particle concentration, pH and natural organic matter. *Sci. Total Environ.* **2009**, *407* (6), 2093−2101.
(77) Daugherty, E. E.; Gilbert, B.; Nico, P. S.; Borch, T. Complexation and Redox Buffering of Iron(II) by Dissolved Organic Matter. *Environ. Sci. Technol.* **2017**, *51* (19), 11096−11104.
(78) Rose, A. L.; Waite, T. D. Kinetics of iron complexation by dissolved natural organic matter in coastal waters. *Mar. Chem.* **2003**, *84* (1), 85−103.

https://dx.doi.org/10.1021/acs.est.0c02959
Environ. Sci. Technol. 2020, 54, 10109−10117